Monthly Notices
of the
ROYAL ASTRONOMICAL SOCIETY

MNRAS **460,** 4063–4074 (2016)
Advance Access publication 2016 May 26

doi:10.1093/mnras/stw1133

ExoMol molecular line lists – XVI. The rotation–vibration spectrum of hot H_2S

Ala'a A. A. Azzam,[1,2] Jonathan Tennyson,[1⋆] Sergei N. Yurchenko[1] and Olga V. Naumenko[3]

[1]*Department of Physics and Astronomy, University College London, London WC1E 6BT, UK*
[2]*Department of Physics, The University of Jordan, Queen Rania Street, Amman 11942, Jordan*
[3]*Institute of Atmospheric Optics, Russian Academy of Sciences, Tomsk 634055, Russia*

Accepted 2016 May 10. Received 2016 May 9; in original form 2016 March 30

ABSTRACT

This work presents the AYT2 line list: a comprehensive list of 115 million $^1H_2{}^{32}S$ vibration–rotation transitions computed using an empirically adjusted potential energy surface and an ab initio dipole moment surface. The line list gives complete coverage up to 11 000 cm^{-1} (wavelengths longer than 0.91 μm) for temperatures up to 2000 K. Room temperature spectra can be simulated up to 20 000 cm^{-1} (0.5 μm) but the predictions at visible wavelengths are less reliable. AYT2 is made available in electronic form as supplementary data to this paper at www.exomol.com.

Key words: molecular data – opacity – astronomical data bases: miscellaneous – planets and satellites: atmospheres.

1 INTRODUCTION

The investigation of the sulphur chemistry in space is a subject of the active research (Russell & Kivelson 2001; Wakelam et al. 2004; Visscher, Lodders & Fegley 2006; Zahnle et al. 2009; Aladro et al. 2011; Hu, Seager & Bains 2013). In particular, Hu et al. (2013) studied the atmospheric composition and the spectra of earth-like exoplanets with sulphur compounds such as hydrogen sulphide (H_2S) and sulphur dioxide (SO_2) using a one-dimensional photochemistry model and associated radiative transfer model to investigate sulphur chemistry in atmospheres ranging from reducing to oxidizing. Visscher et al. (2006) used thermochemical equilibrium and kinetic calculations to model sulphur chemistry in giant planets, brown dwarfs and extrasolar giant planets, and found that H_2S is the dominant S-bearing gas throughout substellar atmospheres and approximately represents the atmospheric sulphur inventory. Therefore, observations of H_2S in these objects should provide a good estimate of their atmospheric sulphur content. H_2S has been, however, ruled out as a potential biosignature in atmospheres of exoplanets according to a biomass-based model study by Seager, Bains & Hu (2013).

H_2S has long been known in the interstellar medium (Thaddeus et al. 1972) and is important in star-forming (Wakelam et al. 2004; Neufeld et al. 2015) and circumstellar (Omont et al. 1993) regions. Aladro et al. (2011) detected H_2S for the first time in galaxy M82, where they studied the chemical complexity towards the central parts of the starburst galaxy, and investigated the role of certain molecules as tracers of the physical processes in the galaxy circumnuclear region. Russell & Kivelson (2001) found evidence for SO_2, SO and H_2S sulphide in Io's exosphere. For Venus, the H_2S composition of the atmosphere at altitudes below 100 km was studied by Von Zahn & Moroz (1985) and de Bergh et al. (2006). Determination of the abundances of gases such as CO, SO_2, OCS, S_2 or H_2S near the surface is important to constrain the oxidation state of the lower atmosphere and surface, and determine the stability of various minerals. Also, measurements at higher altitudes of, for example, SO_3, SO or elemental sulphur are needed to better understand the sulphur cycle and the chemistry at work below the cloud base. Conversely, a recent search for H_2S in volcanic emissions on Mars failed to detect any (Khayat et al. 2015). H_2S is known to be present in comets (Biver et al. 2002) being first detected by Bockelée-Morvan et al. (1991).

On Earth naturally occurring H_2S is associated with volcanic activity (Hoshyaripour, Hort & Langmann 2012). Gaseous H_2S is also detected in a number of other situations including emissions from waste water (Llavador Colomer, Espinos Morato & Mantilla Iglesias 2012) and as a by-product of industrial processes (Szabo et al. 2013).

Known experimental absorption spectra of H_2S molecule cover the region from the microwave up to the visible (0.6 μm). Observations include transitions belonging to 59 vibrational bands associated with different 14 polyads (Polovtseva et al. 2012), where the polyad number is defined as $n = v_1 + v_2/2 + v_3$, where v_i are standard normal mode vibrational quantum numbers.

The rotational band has received attention from many experimentalists (Burrus & Gordy 1953; Huiszoon & Dymanus 1966; Cupp, Keikpf & Gallagher 1968; Miller, Leroi & Hard 1969; Huiszoon 1971; Helminger, Cook & De Lucia 1972; Flaud, Camy-Peyret &

⋆ E-mail: j.tennyson@ucl.ac.uk

Johns 1983; Burenin et al. 1985; Yamada & Klee 1994; Belov et al. 1995; Azzam et al. 2013; Cazzoli, Puzzarini & Gauss 2014). The first bending vibrational band (ν_2) at 1183 cm^{-1} was studied by Lane et al. (1982), Strow (1983) and Ulenikov et al. (1996a). The two fundamental stretching, symmetric (ν_1) and asymmetric (ν_3) lying at 2615 and 2626 cm^{-1}, respectively, are not isolated but overlapped with strong Coriolis and Fermi resonance interactions. The first triad region ($2\nu_2$, ν_1 and ν_3) was studied by Gillis & Edwards (1981), the second triad region ($3\nu_2$, $\nu_1 + \nu_2$ and $\nu_2 + \nu_3$) was studied by Snyder & Edwards (1969) and Ulenikov et al. (1996b), while Brown et al. (1998) studied these two triad regions simultaneously. The 4500–5600 cm^{-1} spectral region was investigated by Brown et al. (1997). Brown et al. (2004a) and Ulenikov et al. (2005) recorded and analysed the transitions in the region 5700–6600 cm^{-1}. In the 7300–7900 cm^{-1} region, more than 1550 transitions up to $J = 14$ were recorded and analysed by Ulenikov et al. (2004). The absorption spectrum in the region 8400–8900 cm^{-1} was recorded by Brown et al. (2004b). Bykov et al. (1994) recorded and analysed spectra between 2000 and 11 147 cm^{-1}. A number of shorter wavelength regions have been studied, namely 9540–10 000 cm^{-1} by Ding et al. (2003), 10 780–11 330 cm^{-1} by Naumenko & Campargue (2001a), 11 930–12 300 cm^{-1} by Großkloß et al. (1994) and Flaud et al. (1995), 12 270–12 670 cm^{-1} by Vaittinen et al. (1997), near 13 200 cm^{-1} by Campargue & Flaud (1999), 14 100–14 400 cm^{-1} by Flaud, Vaittinen & Campargue (1998) and 16 180–16 440 cm^{-1} by Naumenko & Campargue (2001b). This situation is summarized in Fig. 1.

All this work has been performed using cool samples, which are below 300 K. The highest recorded value of the rotational quantum number J is 22 in the rotational band region, and the highest predicted value is 27 in the same region. Altogether around 10 000 ro-vibrational energy levels are known from these experiments. The spectroscopic data for the H_2S molecule have been used to populate various spectroscopic data bases. Table 1 summarizes the contents of the HITRAN 2012 (Rothman et al. 2013), GEISA (Jacquinet-Husson et al. 2011, 2016), W@DIS (Polovtseva et al. 2012), CDMS (Müller et al. 2001, 2005) and JPL (Pickett et al. 1998) data bases. All these data bases contain data resulting from fitted effective Hamiltonians, apart from W@DIS which contains only measured transitions without intensities. The 2012 release of HITRAN (Rothman et al. 2013) updated HITRAN 2008 (Rothman et al. 2009) using extra data on the rotational band of H_2S from Azzam et al. (2013) and the data published in IAO LMS Spectra (spectra.iao.ru).

While absorption spectra of H_2S at elevated temperature have recently been recorded in the ultraviolet by Grosch, Fateev & Clausen (2015), we are unaware of any high-resolution experimental studies of H_2S infrared spectra at higher than ambient temperature. H_2S cross-sections have been measured up to $T = 50$ C as part of PNNL data base (Sharpe et al. 2004).

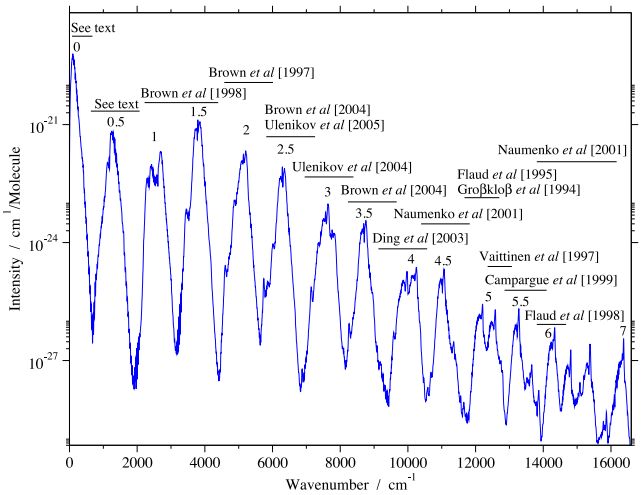

Figure 1. Summary of experimental work on the H_2S absorption spectrum overlaid with our theoretical cross-sections. All spectra were recorded at room temperature. The polyad number of each band is also given.

A number of theoretical studies have considered H_2S. Its ro-vibrational spectrum was calculated by Senekowitsch et al. (1989), Tarczay et al. (2001) and Tyuterev et al. (2004). In the work of Senekowitsch et al. (1989), the room temperature absorption ro-vibrational spectrum of H_2S was calculated variationally for the pure rotational and ν_2, $2\nu_2$, ν_1 and ν_3 transitions from $J = 0$ to 13, where the full account of the anharmonicity effects and ro-vibration couplings was considered. Senekowitsch et al. (1989) calculated the vibrational band origins of the fundamental transitions with accuracy better than 10 cm^{-1}, and the ro-vibrational transitions to within a few tenths of a cm^{-1} for low J's and up to a few cm^{-1} for high J's; their work was also extended to deuterated isotopologues (Miller et al. 1990). The anomalies in the spectral intensity for this molecule were obtained qualitatively. Tarczay et al. (2001) calculated the vibrational band origins of $H_2{}^{32}S$ with accuracy of 29 cm^{-1} up to 14 300 cm^{-1}, and the rotational transitions of the ground vibrational state for $J = 17$ with deviations from the experimental values from 2 to 10 cm^{-1}. Tyuterev et al. (2004) used a spectroscopically determined potential energy surface (PES) to compute the spectrum in the interval 0–8000 cm^{-1}, for J up to 18 and with an intensity

Table 1. Summary for the H_2S spectral data available in different data bases.

Data base	Isotopologue	Bands #	Transitions #	Wavenumber$_{min}$ (cm^{-1})	Wavenumber$_{max}$ (cm^{-1})
HITRAN 2012	$H_2{}^{32}S$	49	36 561	2	11 330
	$H_2{}^{33}S$	19	6322	5	11 072
	$H_2{}^{34}S$	24	11 352	5	11 227
GEISA	$H_2{}^{32}S$	14	12 330	2	4257
	$H_2{}^{33}S$	8	3564	5	4098
	$H_2{}^{34}S$	8	4894	5	4171
W@DIS	$H_2{}^{32}S$	59	34 148	1	16 437
CDMS	$H_2{}^{32}S$	1	1501	1	554
	$H_2{}^{33}S$	1	4759	1	402
	$H_2{}^{34}S$	1	990	1	444
JPL	$H_2{}^{32}S$	1	1525	1	333

cut-off $\leq 10^{-27}$ cm^{-1}/(molecule$\times$cm^{-2}); they reported calculated transitions to be better than 0.01 cm^{-1} for the line positions and 1–3 per cent in the intensities for the strong and medium lines and to $\sim$10 per cent for the weak lines for room temperature conditions. Very recently, Carvajal & Lemus (2015) explored the use of ladder operators to study the vibrational spectrum of this system.

Remote detection of H_2S relies on well-characterized laboratory spectra. At higher temperatures, the resulting list of transitions becomes very extensive and is best calculated using a robust theoretical model (Tennyson 2012). The ExoMol project (Tennyson & Yurchenko 2012) aims to provide molecular line lists for exoplanet and other atmospheres with a particular emphasis on hot species. In this work, we present a comprehensive, hot line list of vibration–rotation transitions of $^1H_2{}^{32}S$. This line list should be appropriate for temperatures up to 2000 K. The methodology used, which is discussed in the following section, closely follows that used to generate comprehensive hot line lists for triatomic species such as water (Barber et al. 2006; Kyuberis et al. 2016) and, recently, SO_2 (Underwood et al. 2016). Section 3 presents our line list computations. Results and comparisons are given in Section 4. Section 5 gives our conclusions.

2 THEORETICAL METHOD

In order to compute a line list for H_2S, three things are required (Lodi & Tennyson 2010): a suitable PES, dipole moment surfaces (DMS) and a nuclear motion program. Each of these is considered in turn below.

2.1 Potential energy surfaces

Four PESs were tested. Our starting point was an ab initio PES constructed using the CCSD(T)/aug-cc-pV(Q+d)Z level of theory as implemented in MOLPRO (Werner et al. 2012). This surface was fitted to the function form given by Tyuterev, Tashkun & Schwenke (2001) using 1200 geometries covering the energy range up to 40 000 cm^{-1} above equilibrium. The surface was then refined by fitting it to the available experimental values of H_2S for $J \leq 6$ covering the energy range up to 16 500 cm^{-1} with a root-mean-square (rms) error of 0.03 cm^{-1} for the fit. We will call this surface PES-Y. This surface was tested by calculating the energy levels for $J = 0$, 1, 2, 5 and 10, and comparing the results with experimental energy levels.

The second PES, PES-T, was constructed by Tyuterev et al. (2001), using a data set of then-available experimentally determined H_2S energy levels. This surface was obtained by the simultaneous fit of a large sample of high-resolution ro-vibrational data, using an extensive set of more than 12 000 experimental ro-vibrational transitions for seven isotopologues of H_2S. This surface is the most accurate available empirically determined PES. However, using the published parameters of PES-T and calculating the ro-vibrational energy levels, we found some problems. Tyuterev et al. used DVR3D (Tennyson et al. 2004) to confirm the convergence of the basis set used in their work for high vibrational states. First, calculating the vibrational energy levels using PES-T with the parameters suggested for DVR3D by Tyuterev et al. ($r_e = 2.75$, $D_e = 0.1$, $\omega_e = 0.01$, all in au, NPNT2 = 35 and NALF = 98), and then comparing these calculated energy values with the experimental vibrational energy levels taken from Tyuterev et al. (2001), we could not reproduce the values for the vibrational energy levels as published by Tyuterev et al., see Table 2. Secondly, testing PES-T for convergence shows that increasing the number of the radial points, NPTN2, some of the energy levels become negative. Graphical investigations showed that this surface develops a hole when the atoms all lie close together. This problem was solved by considering the coefficients up to the quadratic order and ignoring the coefficients with the higher orders in the refining function for the energies above 50 000 cm^{-1}. The modified PES-T was used to calculate the vibrational energy levels again. A further problem is that we found Tyuterev et al.'s vibrational basis set is not converged above 9000 cm^{-1}.

Table 2. Comparison between the experimental and the calculated vibrational levels in cm^{-1}. Columns 1 and 2 give quantum numbers in normal and local modes. Column 3 gives observed vibrational band origins, see Tyuterev et al. (2001); column 4 gives the residuals of these band origins published by Tyuterev et al. (2001); column 5 gives the residuals of the band origins computed using PES-T with the DVR3D parameters suggested by Tyuterev et al. (2001); column 6 gives residuals of the band origins computed using PES-Y0125 and our parameters for DVR3D.

Normal	Local	Obs.	Obs.-Calc.		
($\nu_1\nu_2\nu_3$)	[n_1 $n_3^{\pm}$,b]	3	4	5	6
(010)	[00$^+$,1]	1182.58	−0.01	−0.01	0.02
(020)	[00$^+$,2]	2353.96	0.00	−0.01	−0.02
(100)	[10$^+$,0]	2614.41	−0.02	−0.01	0.06
(030)	[00$^+$,3]	3513.79	0.00	0.00	−0.13
(110)	[10$^+$,1]	3779.17	0.00	0.00	−0.11
(040)	[00$^+$,4]	4661.68	−0.01	0.00	−0.35
(120)	[10$^+$,2]	4932.70	0.01	0.01	−0.16
(200)	[20$^+$,0]	5144.99	−0.01	0.02	0.07
(002)	[11$^+$,0]	5243.10	−0.02	−0.01	0.05
(050)	[00$^+$,5]	5797.24	0.01	0.01	−0.69
(130)	[10$^+$,3]	6074.58	−0.04	−0.04	−0.23
(210)	[20$^+$,1]	6288.15	0.04	0.07	0.05
(102)	[30$^+$,0]	7576.38	−0.03	0.04	0.02
(300)	[21$^+$,0]	7752.26	−0.01	0.02	0.15
(112)	[30$^+$,1]	8697.14	−0.01	0.06	0.08
(202)	[40$^+$,0]	9911.02	0.00	0.18	0.04
(400)	[31$^+$,0]	10 188.30	−0.01	0.06	0.12
(212)	[40$^+$,1]	11 008.68	−0.05	0.13	−0.02
(302)	[50$^+$,0]	12 149.46	0.04	0.40	0.21
(104)	[41$^+$,0]	12 524.63	0.01	0.19	0.07
(312)	[50$^+$,1]	13 222.77	0.05	0.42	−0.22
(322)	[50$^+$,2]	14 284.71	0.02	0.42	−0.74
(402)	[60$^+$,0]	14 291.12	0.03	0.66	0.58

PES-T was further refined using updated experimental levels lying up to 17 000 cm^{-1}; 71 parameters were fitted in two different refinements: (1) using experimental energy levels with $J = 0$, 1, 2 and 5; (2) using experimental energy levels with $J \leq 6$. The resulting two PESs will be referred to as PES-Y0125 and PES-Y0-6, respectively. Convergence tests were performed also for these new refined surfaces by calculating ro-vibrational energy levels for $J =$ 0, 1, 2, 5 and 10, and comparing the calculated values with the available experimental data. PES-Y0125 gives better results than PES-Y0-6. Some results for $J = 0$ are shown in Table 2.

PES-Y0125 predicts experimentally known energy levels with $J \leq 10$ with a standard deviation of 0.11 cm^{-1} compared to 0.23 cm^{-1} using PES-T (using our parameters for DVR3D). Note that Tyuterev et al. claimed that their PES predicted the experimentally known levels with $J \leq 15$ with a standard deviation of 0.03 cm^{-1} for all isotopologues. Table 3 shows the standard deviations for the calculated ro-vibrational energy levels up to 17 000 cm^{-1} using PES-T and PES-Y0125 for $J = 0$, 1, 2, 5 and 10. These calculations show that using PES-Y0125, around 7 per cent of the ro-vibrational energy level with $J \leq 5$ values have errors more than 0.25 cm^{-1}. All of these levels lie above 12 450 cm^{-1}. This proportion increases

Table 3. Standard deviation values of the ro-vibrational energy levels up to 17 000 cm^{-1} for $J = 0$, 1, 2, 5 and 10.

J	Standard deviation (cm^{-1}) PES-Y0125	PES-T
0	0.19	0.24
1	0.06	0.21
2	0.07	0.21
5	0.07	0.23
10	0.19	0.24

with J so that 26 per cent of levels are more than 0.25 cm^{-1} away from the observed $J = 10$ levels, all of them above 8600 cm^{-1}. PES-Y0125 was adopted for this study.

2.2 Dipole moment surfaces

The preferred method of generating accurate intensities is to use ab initio DMS (Lynas-Gray, Miller & Tennyson 1995; Tennyson 2014; Polyansky et al. 2015). However, H_2S intensities are known to be particularly difficult to reproduce since they display a number of anomalies. For example, the observed intensities of all the fundamental bands of H_2S are two-to-three orders of magnitude weaker than those in similar triatomics such as H_2O and H_2Se, and are also much weaker than those of combination bands ($\nu_1 + \nu_2$, $\nu_2 + \nu_3$ and $\nu_1 + \nu_3$; Brown et al. 1998). In particular, the usually strong asymmetric stretch fundamental band ν_3 is even weaker than the $2\nu_2$ bending overtone. Furthermore, all fundamental bands show intensity anomalies in their rotational distributions (Gillis & Edwards 1981; Strow 1983; Brown et al. 1998). For the ν_3 band, some 'forbidden' $\Delta K_a = \pm 2$ transitions are actually more intense than the corresponding 'allowed' $\Delta K_a = 0$ transitions (Brown et al. 1998). Reproducing this behaviour ab initio therefore represents a considerable challenge. Ab initio DMS have been calculated for H_2S by Senekowitsch et al. (1989), by Cours, Tyuterev and co-workers (Cours, Rosmus & Tyuterev 2000, 2002; Henon, Cours & Tyuterev 2003) and us (Azzam et al. 2015).

In this work, we use the ALYT2013 DMS of Azzam et al. (2015) which uses a CCSD(T)/aug-cc-pV(6+d)Z level of theory supplemented by a core-correlation/relativistic corrective surface obtained at the CCSD[T]/aug-cc-pCV5Z-DK level. The intensities computed with this surface agree to within 10 per cent when compared with directly measured experimental data. Further details can be found in Azzam et al. (2015).

2.3 Nuclear motion calculations

Ro-vibrational spectra were computed using the DVR3DR program suite (Tennyson et al. 2004) in Radau coordinates and a bisector embedding. Analysis showed that the published version DVR3DR used a very significant amount of time constructing the final Hamiltonian matrix in module ROTLEV3B. ROTLEV3B uses vibrational functions generated in the first step of the calculation (Tennyson & Sutcliffe 1986) to provide basis functions for the full ro-vibrational calculation performed by ROTLEV3B. For high-J calculations, this algorithm involves transforming a large number of off-diagonal matrix elements to the vibrational basis set representation, see equation 31 in Tennyson & Sutcliffe (1992). This step can be refactored as two successive summations rather than a double summation. The savings in doing this proved to be very significant, so much so that computing the hot ATY2 line list was actually much quicker than generating the original (unpublished) small ATY1 room temperature line list.

Table 4. Input parameters for DVR3DRJZ and ROTLEV3B modules of DVR3D (Tennyson et al. 2004).

Parameter	Value	Description
DVR3DRJZ		
NPNT2	40	No. of radial DVR points (Gauss–Laguerre)
NALF	48	No. of angular DVR points (Gauss–Legendre)
NEVAL	2000	No. of eigenvalues/eigenvectors required
MAX3D	6000	Dimension of final vibrational Hamiltonian
XMASS (S)	31.972 071 Da	Mass of sulphur atom
XMASS (H)	1.007 825 Da	Mass of oxygen atom
r_e	3.8 a_0	Morse parameter (radial basis function)
D_e	0.4 E_h	Morse parameter (radial basis function)
ω_e	0.005 au	Morse parameter (radial basis function)
ROTLEV3B		
NVIB	1400	No. of vib. functions used for each K

Considerable care was taken to ensure convergence of the final calculations, see Azzam (2013) for details. Table 4 gives the parameters used in the final calculation which is sufficient to converge all energy levels considered to about 0.2 cm^{-1}, and very much better than this for the vast majority of them.

3 LINE LIST CALCULATIONS

The calculations for the ATY2 were performed using 16 processors on the machine Amun which are Intel(R) Xeon(R) CPU E7340 @ 2.40GHz. All states with $J \leq 40$ lying up to 21 000 cm^{-1} above the vibrational ground state were included. Einstein A coefficients were generated by considering all transitions involving lower states below 10 000 cm^{-1}. As discussed below, this means that the AYT2 line list is complete at higher temperatures for transition wavenumbers up to 11 000 cm^{-1}. At lower temperatures, it is complete to higher wavenumbers, about 20 000 cm^{-1} at 296 K. The full line list has 115 530 373 lines sorted by frequency and split into 20 files in 1000 cm^{-1} portions.

Table 5 gives a portion of the H_2S state file. DVR3D does not provide approximate quantum numbers: K_a, K_c or the normal mode vibrational labels ν_1, ν_2 and ν_3. Lower lying levels were checked and assigned quantum numbers on the basis of comparison with effective Hamiltonians. For higher levels below about 16 000 cm^{-1}, labels were taken from calculations performed with TROVE (Yurchenko, Thiel & Jensen 2007) and used the correlation between DVR3D and TROVE. The higher stretching states of H_2S are actually better represented by local mode (Jensen 2012) rather than normal mode quantum numbers. However, since there is a one-to-one correspondence between these two representations for XH_2 molecules (Carleer et al. 1999), we simply use the normal mode representation. We note that these quantum numbers are approximate and may be updated in future as better estimates become available. The table also includes a column which gives the calculated radiative decay lifetime for each state. This is a new feature in the ExoMol file structures (Tennyson, Yurchenko & the ExoMol team 2016a). Table 6 gives a portion of the ATY2 transitions file.

Table 5. Extract from the state file for H_2S. The full table is available from http://cdsarc.u-strasbg.fr/cgi-bin/VizieR?-source=J/MNRAS/xxx/yy.

i	$\tilde{E}$	g	J	τ	Γ	K_a	K_c	ν_1	ν_2	ν_3
1	0.000 000	1	0	inf	A1	0	0	0	0	0
2	1182.569 618	1	0	2.2209E+01	A1	0	0	0	1	0
3	2353.907 317	1	0	9.9513E+00	A1	0	0	0	2	0
4	2614.394 829	1	0	1.5263E+01	A1	0	0	1	0	0
5	3513.705 072	1	0	5.1249E+00	A1	0	0	0	3	0
6	3779.189 348	1	0	1.0827E+00	A1	0	0	1	1	0
7	4661.605 794	1	0	2.7037E+00	A1	0	0	0	4	0
8	4932.688 937	1	0	5.7855E-01	A1	0	0	1	2	0
9	5145.031 868	1	0	2.2070E+00	A1	0	0	2	0	0
10	5243.158 956	1	0	2.7018E+00	A1	0	0	0	0	2
11	5797.207 552	1	0	1.4956E+00	A1	0	0	0	5	0
12	6074.566 059	1	0	3.9968E-01	A1	0	0	1	3	0
13	6288.134 723	1	0	4.0625E-01	A1	0	0	2	1	0
14	6385.320 930	1	0	3.4910E-01	A1	0	0	0	1	2
15	6920.081 316	1	0	8.8597E-01	A1	0	0	0	6	0
16	7204.435 162	1	0	3.0530E-01	A1	0	0	1	4	0

i: state counting number.
$\tilde{E}$: state energy in cm^{-1}.
g: state degeneracy.
J: total angular momentum.
τ: state lifetime in s^{-1}, see Tennyson et al. (2016b).
Γ: symmetry.
K_a: asymmetric top quantum number.
K_c: asymmetric top quantum number.
ν_1: symmetric stretch quantum number.
ν_2: bending quantum number.
ν_3: asymmetric stretch quantum number.

Table 6. Extract from the transitions file for H_2S. The full table is available from http://cdsarc.u-strasbg.fr/cgi-bin/VizieR?-source=J/MNRAS/xxx/yy.

f	i	A_{fi}
54 311	54 310	8.2902e−04
96 461	90 862	7.0642e−10
95 160	95 159	2.9992e−04
182 973	182 972	6.2635e−13
66 321	66 320	8.0872e−08
63 788	54 387	1.4876e−09
166 858	166 857	4.1485e−09
66 292	66 291	1.4730e−07
118 595	119 927	3.3674e−08
12 533	9738	2.2129e−02
67 918	67 917	2.2181e−02
19 633	14 097	7.6778e−05
44 469	44 468	1.8778e−12
41 993	41 992	2.5145e−06
64 167	58 776	8.1489e−13
49 157	41 344	3.7880e−01
44 472	39 869	3.7880e−01
183 309	183 308	1.2889e−11
49 527	49 526	3.3570e−10
86 003	80 100	9.6741e−12
31 768	31 767	1.8568e−04

f: upper state counting number.
i: lower state counting number.
A_{fi}: Einstein A coefficient in s^{-1}.

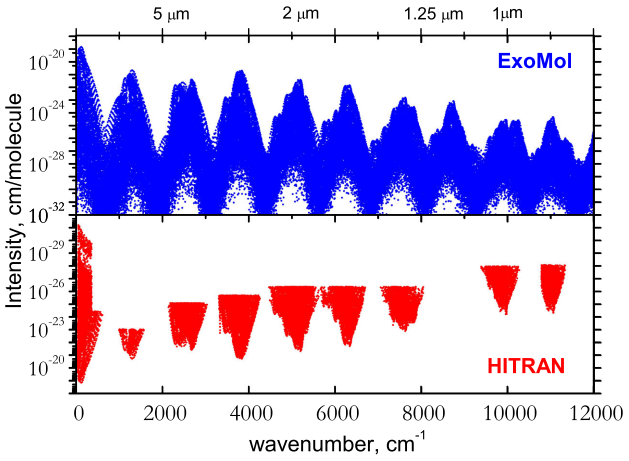

Figure 2. A $T = 296$ K absorption spectrum of H_2S: comparison with HITRAN 2012.

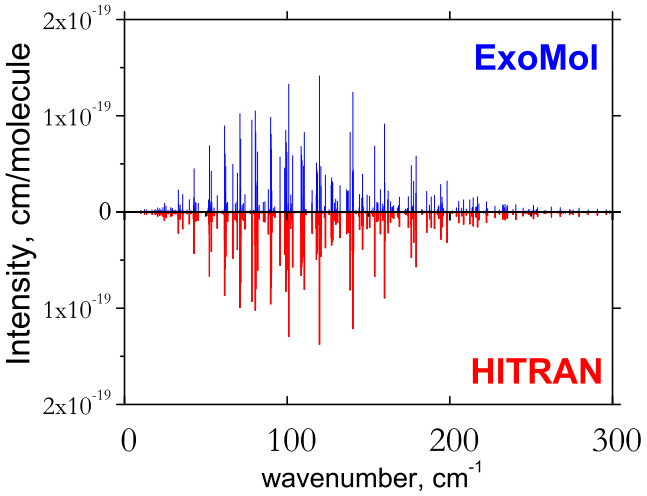

Figure 3. A calculated rotational band compared to that from the HITRAN data base at $T = 296$ K.

3.1 Room temperature comparisons

The accuracy of the calculated spectrum can be checked by comparing the transition positions and intensities with their counterparts in the literature and the data bases. The only available experimental data for H_2S spectra are at room temperature ($T = 296$ K), so we judge the accuracy of our calculations using the spectrum calculated at this temperature. This is not always straightforward for two reasons. First, in order to compare spectra in detail, full assignments are required for the transitions and this is not the case for the calculated transitions using DVR3D. Secondly, our dipole study (Azzam et al. 2015) showed that agreement between our calculations and experimentally measured transitions is much better than with transitions which are the result of (effective Hamiltonian) predictions. As a result, during the comparison, we distinguish between the experimental and predicted transitions.

As a preliminary comparison, Fig. 2 gives a general idea about the number of transitions available in HITRAN 2012 (Rothman et al. 2013) compared to the number of transitions calculated in this work at room temperature. Also, Figs 3 and 4 give a general idea about the accuracy of our calculated line list (ATY2) compared to the data

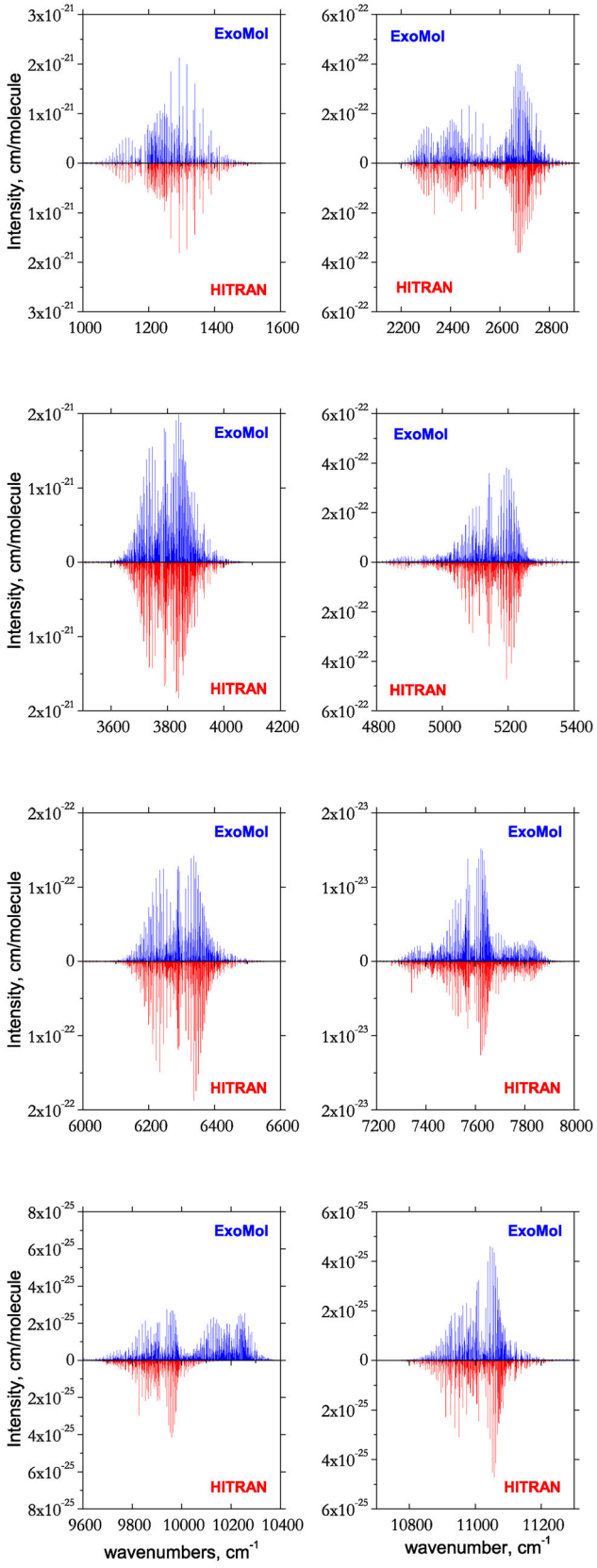

Figure 4. Calculated spectrum at $T = 296$ K compared to that from the HITRAN data base for the polyads (top left to bottom right) 0.5, 1, 1.5, 2, 2.5, 3, 4 and 4.5.

in these data bases; more detailed comparisons are presented in the following subsections.

The data available in HITRAN 2012 for $H_2{}^{32}S$ comprise 36 533 transitions in the spectral region 2–11 330 cm^{-1} and cover J values up to 30 and cut-off intensity of the order of 10^{-32} $cm^{-1}/(molecule \times cm^{-2})$ at 296 K. Our comparisons prioritize actual measured line positions and intensities, which we identified from the data given in HITRAN using additional information provided by the IS WADIS (wadis.saga.iao.ru) data base. A summary of the comparison between our calculations and the data in HITRAN data base for every polyad region is presented in Tables 7–9.

3.1.1 HITRAN data base: 0–4200 cm^{-1}

HITRAN 2012 contains around 14 700 transitions in the 0–4250 cm^{-1} spectral region with an intensity cut-off of the order of 10^{-32} below 360 cm^{-1} and 10^{-26} $cm^{-1}/(molecule \times cm^{-2})$ above 360 cm^{-1}. Of all data provided by the HITRAN 2012 in this region, only around 10 700 transitions with positions either measured or accurately determined from the upper and lower experimental energy levels are included in our comparison. In addition, about 550 simulated transitions of the 010–000 band between 1000 and 1570 cm^{-1} were also used, as no other data are available in HITRAN 2012 for this region. It should be noted that all intensities provided by the HITRAN below 4250 cm^{-1} are calculated values. Fig. 5 shows the differences between ATY2 and HITRAN 2012 in this region for both transition frequencies and intensities. A summary of the comparison between our calculations and the HITRAN data for polyad 0 to 1.5 is presented in Tables 7– 8.

For the pure rotational region 0–360 cm^{-1} (000–000 and 010–010 transitions), the standard or rms deviation between the calculated and measured (Flaud et al. 1983; Azzam et al. 2013) positions up to $J = 26$ is 0.016 cm^{-1} for 1815 observed lines with maximum absolute deviation of 0.094 cm^{-1}. All the intensities in this region are calculated using the permanent dipole moment. Both sets of calculated intensities provided by HITRAN and variational agree very well with an rms of 5.7 per cent and average ratio of 1.04.

Positions of the 010–000 band (polyad 0.5) in HITRAN were simulated based on the spectroscopic parameters reported by Lane et al. (1982) and then normalized to the measured values of Strow (1983). Comparison with AYT2 yields an rms and maximal deviations for line positions of 0.049 and 0.258 cm^{-1}. Variational intensities for the 010–000 band differ significantly from a simulation adopted in HITRAN with an rms deviation of 30 per cent. Measured intensities of 103 lines of the 010–000 band reported by Strow (1983) deviate from variational values within an rms of 23 per cent. The integrated variational intensity of the 010–000 band is about 17 per cent larger than that estimated from HITRAN. This is in agreement with tests for $J \leq 5$ made previously by Azzam et al. (2015).

For the 2140–4250 cm^{-1} spectral region, our comparison was limited to 7505 'empirical' transitions. Similar rms and maximum deviations around 0.07 and 0.36 cm^{-1}, respectively, have been obtained between 'empirical' and calculated positions for polyads 1 and 1.5. In this comparison, we used corrected set of the transition positions above 2000 cm^{-1} which corresponds to the original data of Brown et al. (1998). These data are available in the GEISA-2015 data base (Jacquinet-Husson et al. 2016).

Above 2200 cm^{-1}, the transition intensities adopted in HITRAN are taken from an effective Hamiltonian based on about 1100 accurate (within 2–5 per cent) measured intensities reported by Brown et al. (1998). Comparison of the AYT2 intensities with the HITRAN

Table 7. Comparison between the calculated transitions and the data available in HITRAN for the polyad regions 0 and 0.5. σ is the standard deviation. Absolute intensities are in $cm^{-1}/(molecule \times cm^{-2})$ (powers of 10 in parentheses) and errors are all relative; the frequency errors are absolute errors. The HITRAN data are divided between directly measured and predicted from effective Hamiltonians.

Polyad	Frequency			Intensity	
		Measured		Predicted	Measured
0	Spectral range	3–360 cm^{-1}	Intensity range	1.53(−26)–9.91(−20)	
	J range	1–26	Average ratio	1.04	
	K_a range	0–17	σ	5.7 per cent	
	σ	0.016 cm^{-1}	Min. ratio	0.88	
	Max. deviation	0.094 cm^{-1}	Max. ratio	1.38	
	Total no. of lines	1185		1185	
0.5	Spectral range	994–1573 cm^{-1}	Intensity range	9.10(−24)–1.81(−21)	1.52(−24)–8.34(−21)
	J range	1–16	Average ratio	0.93	0.90
	K_a range	0–14	σ	30 per cent	23 per cent
	σ	0.016 cm^{-1}	Min. ratio	0.43	0.64
	Max. deviation	0.094 cm^{-1}	Max. ratio	1.75	1.88
	Total no. of lines	551		551	103

Table 8. Comparison between the calculated transitions and the data available in HITRAN for the polyad regions 1 and 1.5. σ is the standard deviation. Absolute intensities are in $cm^{-1}/(molecule \times cm^{-2})$ (powers of 10 in parentheses) and errors are all relative; the frequency errors are absolute errors. The HITRAN data are divided between directly measured and predicted from effective Hamiltonians.

Polyad	Frequency			Intensity	
		Empirical		Predicted	Measured
1	Spectral range	2142–3034 cm^{-1}	Intensity range	8.07(−26)–3.61(−22)	5.90(−25)–2.73(−22)
	J range	0–20	Average ratio	1.03	0.99
	K_a range	0–14	σ	17.9 per cent	8.2 per cent
	σ	0.070 cm^{-1}	Min. ratio	0.36	0.55
	Max. deviation	0.338 cm^{-1}	Max. ratio	3.18	1.39
	Total no. of lines	3453		3413	568
1.5	Spectral range	3312–4250 cm^{-1}	Intensity range	2.04(−26)–1.83(−21)	4.89(−25)–1.77(−21)
	J range	0–20	Average ratio	1.09	1.02
	K_a range	0–15	σ	15.6 per cent	7.5 per cent
	σ	0.072 cm^{-1}	Min. ratio	0.54	0.88
	Max. deviation	0.358 cm^{-1}	Max. ratio	3.06	1.35
	Total no. of lines	4050		4026	526

data and accurate measured values is summarized in Table 7 and is illustrated in Fig. 5. Reasonable agreement between the measured and variational intensities with an rms of 8 per cent is achieved, while the predicted HITRAN intensities deviate from the AYT2 predictions by about 16–18 per cent.

3.1.2 HITRAN data base: 4400–8000 cm^{-1}

The H_2S transitions in the 4400–8000 cm^{-1} region represent measured positions and intensities which are augmented with 'empirical' transitions generated from experimental energy levels and intensities predicted using an effective Hamiltonian. Of 16 284 transitions included in HITRAN 2012, 11 277 correspond to observed data. It should be noted that majority of the measured intensities are of low accuracy, often derived from a peak absorption. However, for about 2500 transitions between 4580 and 6575 cm^{-1}, accurate intensities are provided.

Only observed data were used in comparison with variational calculation. A summary of this comparison is given in Table 8 and Fig. 6. The observed positions are reproduced with an rms of 0.08 cm^{-1} (polyad 2.5) and 0.13 cm^{-1} (polyads 2 and 3) with maximal deviations not exceeding 0.6 cm^{-1}.

Intensity comparisons are not so straightforward with strongly distorted ratios between observed and AYT2 intensities for individual transitions. Sometimes this disagreement is due to missing additional lines, or due to incorrect assignment, sometimes the experimental line is a superposition with another H_2S isotopologue, removed from the list. There is also the possibility of increased errors in the AYT2 intensities for individual vibrational bands, due to problems with the DMS, or for individual transitions, due to perturbations (Lodi & Tennyson 2012; Zak et al. 2016). The distribution of intensity ratios was examined for every polyad, and the suitable upper and lower limits chosen which included 91–95 per cent of the lines; these were used to determine the rms deviations presented in Table 8.

The best intensity agreement, with an rms of 6.9 per cent, was obtained for the accurate 1423 experimental intensities for polyad 2, while the rms for all observed lines for this polyad was about 25 per cent. At the same time, intensities of transitions belonging to polyad 2.5 deviated from their AYT2 analogues, see Table 9 and Fig. 6, both for approximate and accurate measured data: of 1084 accurate intensities, only 1019 could be reproduced with an rms of 14 per cent. We note that our calculations appear to overestimate the strength of the $5\nu_2$ band, which lies at about 5800 cm^{-1}, by approximately a factor of 2. This is almost certainly caused by residual problems with DMS of Azzam et al. (2015).

Table 9. Comparison between the calculated transitions and the data available in HITRAN for the polyad regions 2–4.5. σ is the standard deviation. Absolute intensities are in $cm^{-1}/(molecule \times cm^{-2})$ (powers of 10 in parentheses) and errors are all relative; the frequency errors are absolute errors. The HITRAN data are divided between accurately and approximately measured.

Polyad		Frequency		Intensity		
		Measured		Approx. measured	Measured	
2	Spectral range	4486–5595 cm^{-1}	Intensity range	1.88(−26)–4.72(−22)	4.26(−26)–4.09(−22)	
	J range	0–20	Average ratio	1.08	1.01	
	K_a range	0–14	σ	24.8 per cent	6.9 per cent	
	σ	0.127 cm^{-1}	Min. ratio	0.50	0.76	
	Max. deviation	0.524 cm^{-1}	Max. ratio	3.00	1.38	
	Total no. of lines	5617		5165	1423	
2.5	Spectral range	5688–6653 cm^{-1}	Intensity range	1.60(−26)–1.87(−22)	2.11(−26)–1.87(−22)	
	J range	0–18	Average ratio	1.12	1.05	
	K_a range	0–14	σ	32.3 per cent	14.0 per cent	
	σ	0.078 cm^{-1}	Min. ratio	0.40	0.71	
	Max. deviation	0.293 cm^{-1}	Max. ratio	3.00	1.50	
	Total no. of lines	3153		3014	1019	
3	Spectral range	7096–7995 cm^{-1}	Intensity range	1.63(−26)–1.26(−23)		
	J range	0–17	Average ratio	0.99		
	K_a range	0–10	σ	33.8 per cent		
	σ	0.129 cm^{-1}	Min. ratio	0.50		
	Max. deviation	0.358 cm^{-1}	Max. ratio	3.00		
	Total no. of lines	2504		2327		
4	Spectral range	9541–10 001 cm^{-1}	Intensity range	2.98(−28)–6.09(−25)		
	J range	0–17	Average ratio	1.48		
	K_a range	0–11	σ	54 per cent		
	σ	0.138 cm^{-1}	Min. ratio	0.25		
	Max. deviation	0.670 cm^{-1}	Max. ratio	3.95		
	Total no. of lines	1716		1568		
4.5	Spectral range	10 790–11 298 cm^{-1}	Intensity range	2.67(−28)–4.72(−25)		
	J range	0–19	Average ratio	1.48		
	K_a range	0–11	σ	56 per cent		
	σ	0.086 cm^{-1}	Min. ratio	0.27		
	Max. deviation	0.580 cm^{-1}	Max. ratio	2.86		
	Total no. of lines	1093		1015		

3.1.3 HITRAN data base: 9500–11 300 cm^{-1}

The HITRAN 2012 data for H_2S in this region comprise the measurements of Naumenko & Campargue (2001a) and Naumenko & Campargue (2001b) augmented by the calculated lines with 'empirical' positions and intensities predicted on the basis of an effective Hamiltonian model. Of 5605 transitions, only 2835 have measured positions and intensities. Experimental intensities were estimated to be accurate to 25–30 per cent on average and up to 100 per cent for the weakest lines in polyad 4 region, and as 15 per cent for strong- and medium-intensity lines and up to 50 per cent for weakest lines for polyad 4.5.

Again only measured transitions were used in the comparison. Table 9 summarizes the results of the analysis which are shown graphically in Fig. 7. Agreement between the observed and AYT2 line positions was found to be quite satisfactory with an rms of 0.086 and 0.138 cm^{-1} for polyads 4.5 and 4, respectively, while the maximal deviation does not exceed 0.67 cm^{-1} for both polyads. However, the intensities agree less well than for the lower polyads with an rms of 54–56 per cent when about 90 per cent of lines were compared. Much larger deviations in intensity ratios (up to two orders of magnitude) were also encountered. They may be caused by the low accuracy of the experimental intensities, incomplete or incorrect assignments, or by distortion of the calculated values. It seems that calculated intensities of transitions involving the upper states in the local mode limit are strongly sensitive to the details of the PES, and can change significantly for its different versions.

In general, our calculations agree well with the measured transition intensities where we find the difference of up to about a factor of 3 while much larger differences sometimes up to two-to-three orders of magnitude appear for results derived from effective Hamiltonians (not shown). This analysis suggests that there are problems with the effective Hamiltonian extrapolation; this problem will be analysed elsewhere.

Our calculated spectrum at room temperature contains around 620 000 transitions up to $J = 40$ below 12 000 cm^{-1} with the intensity cut-off 10^{-31} $cm^{-1}/(molecule \times cm^{-2})$ comparing to 36 600 transitions in HITRAN 2012. This spectrum has a standard deviation for the transition positions of about 0.072 cm^{-1} for 94 per cent of the 20 513 most accurate measured lines below 8000 cm^{-1} (see Tables 7– 9). The standard deviation of the ratios of the transition intensities in HITRAN 2012 to the calculated intensities is 10 per cent with an average ratio of 1.02 for 76 per cent of lines considered, provided that the less accurate 010–000 transition intensities were excluded from consideration.

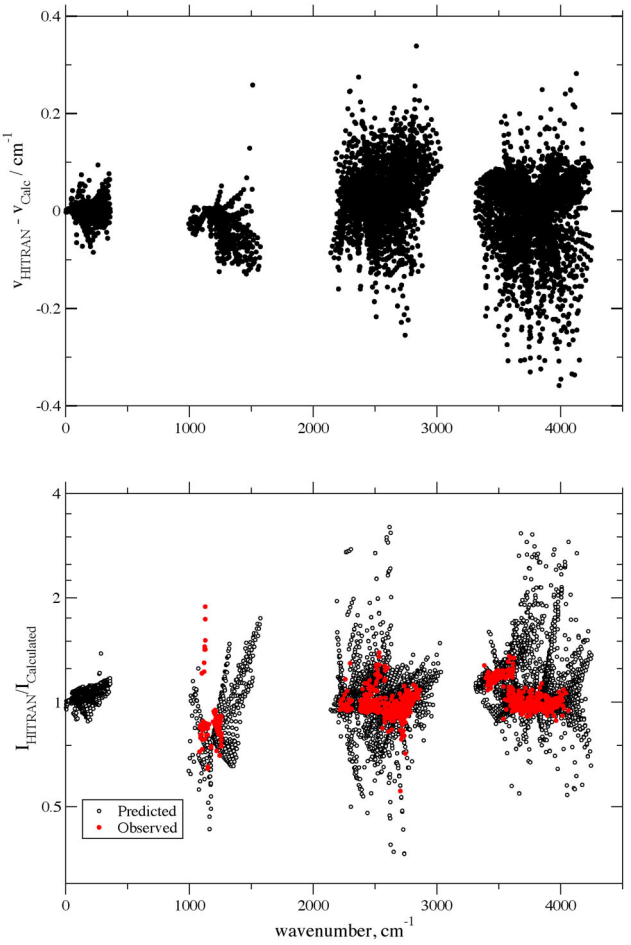

Figure 5. Differences in line positions (upper) and transition intensities (lower) compared to data available in HITRAN below 4000 cm^{-1}. The measured and predicted lines in this data base are considered separately.

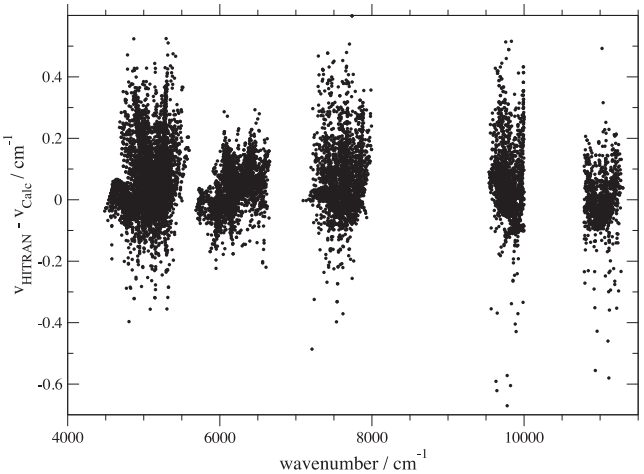

Figure 6. Differences in line positions comparing to actual observed data included in HTRAN2012.

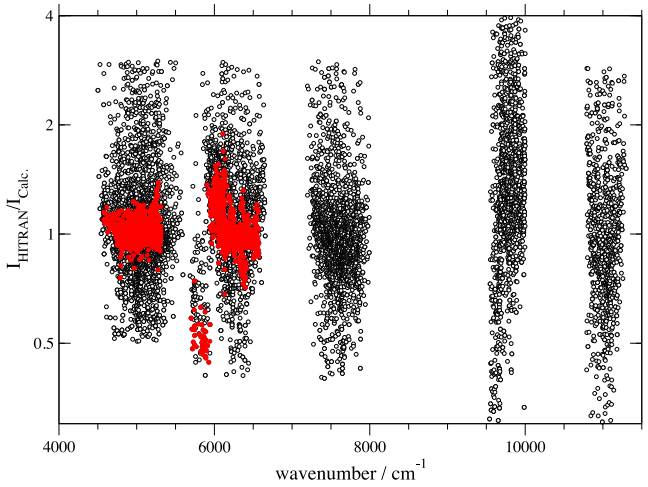

Figure 7. Errors in transition intensities comparing to actual observed data included in HTRAN2012; intensities for which the measurements are accurate are highlighted.

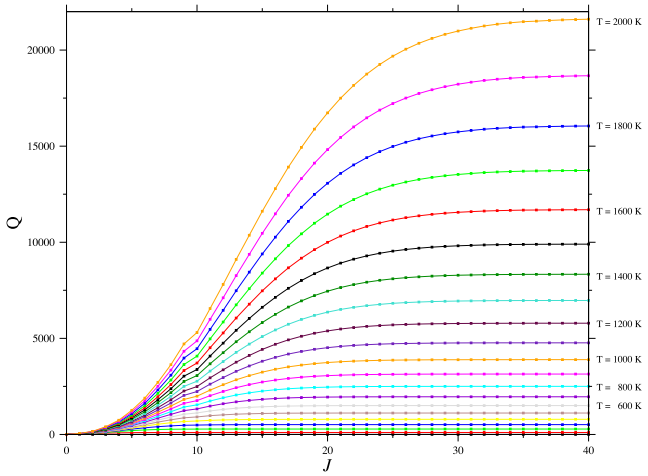

Figure 8. Partition functions' convergence curves.

4 PARTITION FUNCTION AND LIFETIMES

The partition function value (Q) of a molecule at temperature (T) is given by

$$Q(T) = \sum_J \sum_i g_i(2J+1) \exp\left(-\frac{c_2 E_i^{(J)}}{T}\right), \quad (1)$$

where g is the nuclear statistical weight which is 1 or 3 for para or ortho states of $H_2{}^{32}S$ in the convention adopted by HITRAN and ExoMol; $E_i^{(J)}$ is the ro-vibrational energy for a given J value and c_2 is the second radiation constant. The summation in this equation should be performed over all ro-vibrational energy levels or at least until the value of Q converges. Fig. 8 shows how Q converges with J at different temperatures up to 2000 K. Table 10 presents $H_2{}^{32}S$ Q values at different temperatures in comparison with the values from the HITRAN, the JPL (Pickett et al. 1998) and the CDMS data bases.

The lifetimes of H_2S were computed using the Einstein A coefficients from the ATY2 line list following the methodology laid out by Tennyson et al. (2016b). Results are summarized in Fig. 9; we note that the lifetimes are much more regular as a function of

Table 10. $H_2{}^{32}S$ partition function values at different temperatures from different sources.

T/K	This work	HITRAN[a]	JPL[b]
2.725	1.0077		
5	1.2458		
9.375	2.9106		2.9106
18.75	8.6997		8.6996
37.5	23.8654		23.8654
75	65.5266	65.4854	65.5265
100	100.1557	99.972 09	
150	182.7646	182.2696	182.7622
200	280.6278	279.6049	
225	334.6933	333.3219	334.5222
296	505.7921	503.07[c]	
300	516.1942	513.3829	514.4470
400	803.3417	797.6368	
500	1146.2892	1136.46	
600	1552.6512	1537.079	
700	2032.2186	2009.062	
800	2596.5908	2563.217	
900	3258.9381	3211.929	
1000	4033.8404	3968.802	
1100	4937.2034	4848.387	
1200	5986.2329	5866.361	
1300	7199.4423	7039.470	
1400	8596.6730	8385.471	
1500	10 199.1148	9923.019	
1600	12 029.3175	11 672.66	
1700	14 111.1872	13 655.08	
1800	16 469.9578	15 893.10	
1900	19 132.1349	18 409.06	
2000	22 125.4048	21 229.28	

[a]As calculated using the HITRAN's FORTRAN programs for partition function sums.
[b]As published on the JPL's website; values are very similar to those given by CDMS.
[c]From Šimečková et al. (2006).

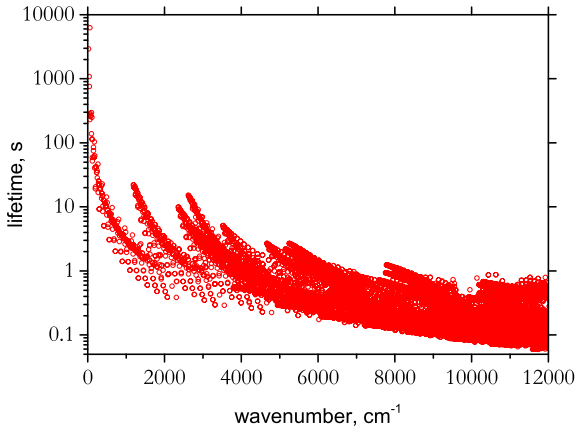

Figure 9. Lifetimes of H_2S obtained using the line list (ATY2).

changes in quantum numbers than those computed by Tennyson et al. (2016b) for water.

5 HOT SPECTRA

Fig. 10 shows the calculated spectra at different temperatures. This figure shows how the weak transitions at low temperatures become stronger at higher temperatures. The spectrum at 2000 K contains

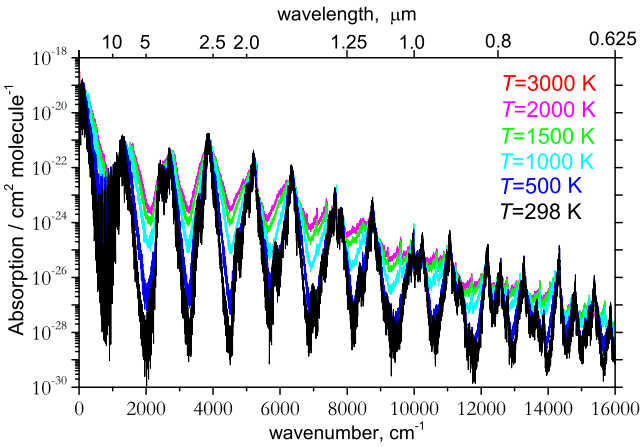

Figure 10. Temperature-dependent spectra generated using the ATY2 line list. The depth of the minima (windows) decreases monotonically with temperature.

46 million transitions up to 12 000 cm^{-1}, with $J \leq 40$ with intensities greater than 10^{-31} cm^{-1}/(molecule$\times$$cm^{-2}$). Transition positions do not change with temperature unlike transition intensities which are temperature dependent due to the $e^{-E_{low}/kT}$ Boltzmann factor. The ATY2 line list can also be used to simulate room temperature spectra up to 20 000 cm^{-1}; however, our calculations are less accurate at visible wavelengths.

No line intensities of H_2S can be found to compare our calculations with, neither experimental nor theoretical with temperatures higher than 296 K. This makes our line list the first available source of data for $H_2{}^{32}S$ spectra at temperatures higher than room temperature, thus, opening the door for the possible identification of $H_2{}^{32}S$ transitions in exoplanet and brown dwarf atmospheres. This line list can also be used in the high-temperature laboratory spectra analysis.

Inspection of Fig. 10 shows that, unusually, the maximum infrared absorption lies at 2.5 μm rather than at longer wavelengths. This is a manifestation of the unusual dipole moment of H_2S which results in the fundamental bands being weaker than the overtones at about 2.5 μm.

6 CONCLUSION

A new hot line list for H_2S, called ATY2, has been computed containing 115 million transitions. The line list is divided into an energy file and a transitions file. This is done using the new ExoMol format (Tennyson et al. 2016a). The full line list can be downloaded from the CDS, via ftp://cdsarc.u-strasbg.fr/pub/cats/J/MNRAS/xxx/yy, or http://cdsarc.u-strasbg.fr/viz-bin/qcat?J/MNRAS//xxx/yy, as well as the ExoMol website, www.exomol.com. The line lists and partition function together with auxiliary data including the potential parameters and dipole moment functions, as well as the absorption spectrum given in cross-section format (Hill, Yurchenko & Tennyson 2013), can all be obtained also from www.exomol.com as part of the extended ExoMol data base (Tennyson et al. 2016a).

ACKNOWLEDGEMENTS

This work was supported by the ERC under the Advanced Investigator Project 267219 and the University of Jordan. JT and SNY thank the support of the COST action MOLIM (CM1405).

We thank the Royal Society for supporting a visit by OVN to London.

REFERENCES

Aladro R., Martin S., Martin-Pintado J., Mauersberger R., Henkel C., Ocana Flaquer B., Amo-Baladron M. A., 2011, A&A, 535, A84

Azzam A. A. A., 2013, PhD thesis, University College London

Azzam A. A. A., Yurchenko S. N., Tennyson J., Martin M.-A., Pirali O., 2013, J. Quant. Spectrosc. Radiat. Transfer, 130, 341

Azzam A. A. A., Lodi L., Yurchenko S. N., Tennyson J., 2015, J. Quant. Spectrosc. Radiat. Transfer, 161, 41

Barber R. J., Tennyson J., Harris G. J., Tolchenov R. N., 2006, MNRAS, 368, 1087

Belov S. P., Yamada K. M. T., Winnewisser G., Poteau L., Bocquet R., Demaison J., Polyansky O., Tretyakov M. Y., 1995, J. Mol. Spectrosc., 173, 380

Biver N. et al., 2002, Earth Moon Planets, 90, 323

Bockelée-Morvan D., Colom P., Crovisier J., Despois D., Paubert G., 1991, Nature, 350, 318

Brown L. R., Crisp J. A., Crisp D., Naumenko O. V., Smirnov M. A., Sinitsa L. N., 1997, Proc. SPIE, 3090, 111

Brown L. R., Crisp J. A., Crisp D., Naumenko O. V., Smirnov M. A., Sinitsa L. N., Perrin A., 1998, J. Mol. Spectrosc., 188, 148

Brown L. R., Naumenko O. V., Polovtseva E. R., Sinitsa L. N., 2004a, Proc. SPIE, 5311, 59

Brown L. R., Naumenko O. V., Polovtseva E. R., Sinitsa L. N., 2004b, Proc. SPIE, 5743, 1

Burenin A. V., Fevralskikh T. M., Melnikov A. A., Shapin S. M., 1985, J. Mol. Spectrosc., 109, 1

Burrus C. A., Jr, Gordy W., 1953, Phys. Rev., 92, 274

Bykov A. D., Naumenko O. V., Smirnov M. A., Sinitsa L. N., Brown L. R., Crisp J., Crisp D., 1994, Can. J. Phys., 72, 989

Campargue A., Flaud J.-M., 1999, J. Mol. Spectrosc., 194, 43

Carleer M. et al., 1999, J. Chem. Phys., 111, 2444

Carvajal M., Lemus R., 2015, J. Phys. Chem. A, 119, 12823

Cazzoli G., Puzzarini C., Gauss J., 2014, A&A, 566, A52

Cours T., Rosmus P., Tyuterev V. G., 2000, Chem. Phys. Lett., 331, 317

Cours T., Rosmus P., Tyuterev V. G., 2002, J. Chem. Phys., 117, 5192

Cupp R. E., Keikpf R. A., Gallagher J. J., 1968, Phys. Rev., 171, 60

de Bergh C., Moroz V. I., Taylor F. W., Crisp D., Bézard B., Zasova L. V., 2006, Planet. Space Sci., 54, 1389

Ding Y., Naumenko O., Hu S.-M., Zhu Q., Bertseva E., Campargue A., 2003, J. Mol. Spectrosc., 217, 222

Flaud J. M., Grosskloss R., Rai S. B., Stuber R., Demtroder W., Tate D. A., Wang L. G., Gallagher T. F., 1995, J. Mol. Spectrosc., 172, 275

Flaud J.-M., Camy-Peyret C., Johns J. W. C., 1983, Can. J. Phys., 61, 1462

Flaud J.-M., Vaittinen O., Campargue A., 1998, J. Mol. Spectrosc., 190, 262

Gillis J. R., Edwards T. H., 1981, J. Mol. Spectrosc., 85, 55

Grosch H., Fateev A., Clausen S., 2015, J. Quant. Spectrosc. Radiat. Transfer, 154, 28

Großkloß R., Rai S. B., Stuber R., Demtroder W., 1994, Chem. Phys. Lett., 229, 609

Helminger P., Cook R. L., De Lucia F. C., 1972, J. Chem. Phys., 56, 4581

Henon E., Cours T., Tyuterev V. G., 2003, Chem. Phys. Lett., 367, 284

Hill C., Yurchenko S. N., Tennyson J., 2013, Icarus, 226, 1673

Hoshyaripour G., Hort M., Langmann B., 2012, Geochem. Geophys. Geosys., 13, Q07004

Hu R., Seager S., Bains W., 2013, ApJ, 769

Huiszoon C., 1971, Rev. Sci. Instrum., 42, 477

Huiszoon C., Dymanus A., 1966, Phys. Lett., 21, 164

Jacquinet-Husson N. et al., 2011, J. Quant. Spectrosc. Radiat. Transfer, 112, 2395

Jacquinet-Husson N. et al., 2016, J. Mol. Spectrosc, in press

Jensen P., 2012, WIREs Comput. Mol. Sci., 2, 494

Khayat A. S., Villanueva G. L., Mumma M. J., Tokunaga A. T., 2015, Icarus, 253, 130

Kyuberis A. A., Polyansky O. L., Lodi L., Tennyson J., Ovsyannikov R. I., Zobov N., 2016, MNRAS

Lane W. C., Edwards T. H., Gillis J. R., Bonomo F. S., Murcray F. J., 1982, J. Mol. Spectrosc., 95, 365

Llavador Colomer F., Espinos Morato H., Mantilla Iglesias E., 2012, J. Air Waste Manage. Assoc., 62, 758

Lodi L., Tennyson J., 2010, J. Phys. B: At. Mol. Opt. Phys., 43, 133001

Lodi L., Tennyson J., 2012, J. Quant. Spectrosc. Radiat. Transfer, 113, 850

Lynas-Gray A. E., Miller S., Tennyson J., 1995, J. Mol. Spectrosc., 169, 458

Miller R. E., Leroi G. E., Hard T. M., 1969, J. Chem. Phys., 50, 677

Miller S., Tennyson J., Rosmus P., Senekowitsch J., Mills I. M., 1990, J. Mol. Spectrosc., 143, 61

Müller H. S. P., Thorwirth S., Roth D. A., Winnewisser G., 2001, A&A, 370, L49

Müller H. S. P., Schlöder F., Stutzki J., Winnewisser G., 2005, J. Mol. Struct., 742, 215

Naumenko O., Campargue A., 2001a, J. Mol. Spectrosc., 209, 242

Naumenko O., Campargue A., 2001b, J. Mol. Spectrosc., 210, 224

Neufeld D. A. et al., 2015, A&A, 577, A49

Omont A., Lucas R., Morris M., Guilloteau S., 1993, A&A, 267, 490

Pickett H. M., Poynter R. L., Cohen E. A., Delitsky M. L., Pearson J. C., Muller H. S. P., 1998, J. Quant. Spectrosc. Radiat. Transfer, 60, 883

Polovtseva E. R., Lavrentiev N. A., Voronina S. S., Naumenko O. V., Fazliev A. Z., 2012, Atmos. Ocean. Opt., 25, 157

Polyansky O. L., Bielska K., Ghysels M., Lodi L., Zobov N. F., Hodges J. T., Tennyson J., 2015, Phys. Rev. Lett., 114, 243001

Rothman L. S. et al., 2009, J. Quant. Spectrosc. Radiat. Transfer, 110, 533

Rothman L. S. et al., 2013, J. Quant. Spectrosc. Radiat. Transfer, 130, 4

Russell C. T., Kivelson M. G., 2001, J. Geophys. Res. Planets, 106, 33267

Seager S., Bains W., Hu R., 2013, ApJ, 775, 104

Senekowitsch J., Carter S., Zilch A., Werner H.-J., Handy N. C., 1989, J. Chem. Phys., 90, 783

Sharpe S. W., Johnson T. J., Sams R. L., Chu P. M., Rhoderick G. C., Johnson P. A., 2004, Appl. Spectrosc., 58, 1452

Šimečková M., Jacquemart D., Rothman L. S., Gamache R. R., Goldman A., 2006, J. Quant. Spectrosc. Radiat. Transfer, 98, 130

Snyder L. E., Edwards T. H., 1969, J. Mol. Spectrosc., 31, 347

Strow L. L., 1983, J. Quant. Spectrosc. Radiat. Transfer, 29, 395

Szabo A., Mohacsi A., Gulyas G., Bozoki Z., Szabo G., 2013, Meas. Sci. Technol., 24, 065501

Tarczay G., Császár A. G., Polyansky O. L., Tennyson J., 2001, J. Chem. Phys., 115, 1229

Tennyson J., 2012, WIREs Comput. Mol. Sci., 2, 698

Tennyson J., 2014, J. Mol. Spectrosc., 298, 1

Tennyson J., Sutcliffe B. T., 1986, Mol. Phys., 58, 1067

Tennyson J., Sutcliffe B. T., 1992, Int. J. Quantum Chem., 42, 941

Tennyson J., Yurchenko S. N., 2012, MNRAS, 425, 21

Tennyson J., Kostin M. A., Barletta P., Harris G. J., Polyansky O. L., Ramanlal J., Zobov N. F., 2004, Comput. Phys. Commun., 163, 85

Tennyson J. et al., 2016a, preprint (arXiv:1603.05890).

Tennyson J., Hulme K., Naim O. K., Yurchenko S. N., 2016b, J. Phys. B: At. Mol. Opt. Phys., 49, 044002

Thaddeus P., Wilson R. W., Kutner M. L., Jefferts K. B., Penzias A. A., 1972, ApJ, 176, L73

Tyuterev V. G., Tashkun S. A., Schwenke D. W., 2001, Chem. Phys. Lett., 348, 223

Tyuterev V. G., Regalia-Jarlot L., Schwenke D. W., Tashkun S. A., Borkov Y. G., 2004, C. R. Phys., 5, 189

Ulenikov O. N., Malikova A. B., Koivusaari M., Alanko S., Anttila R., 1996a, J. Mol. Spectrosc., 176, 229

Ulenikov O. N., Onopenko G. A., Koivusaari M., Alanko S., Anttila R., 1996b, J. Mol. Spectrosc., 176, 236

Ulenikov O. N., Liu A.-W., Bekhtereva E. S., Gromova O. V., Hao L.-Y., Hu S.-M., 2004, J. Mol. Spectrosc., 226, 57
Ulenikov O. N., Liu A.-W., Bekhtereva E. S., Gromova O. V., Hao L.-Y., Hu S.-M., 2005, J. Mol. Spectrosc., 234, 270
Underwood D. S., Tennyson J., Yurchenko S. N., Huang X., Schwenke D. W., Lee T. J., Clausen S., Fateev A., 2016, MNRAS, 459, 3890
Vaittinen O., Biennier L., Campargue A., Flaud J.-M., Halonen L., 1997, J. Mol. Spectrosc., 184, 288
Visscher C., Lodders K., Fegley B., Jr, 2006, A&A, 648, 1181
Von Zahn U., Moroz V. I., 1985, Adv. Space Res., 5, 173
Wakelam V., Castets A., Ceccarelli C., Lefloch B., Caux E., Pagani L., 2004, A&A, 413, 609
Werner H.-J., Knowles P. J., Knizia G., Manby F. R., Schütz M., 2012, WIREs Comput. Mol. Sci., 2, 242
Yamada K. M. T., Klee S., 1994, J. Mol. Spectrosc., 166, 395
Yurchenko S. N., Thiel W., Jensen P., 2007, J. Mol. Spectrosc., 245, 126
Zahnle K., Marley M. S., Freedman R. S., Lodders K., Fortney J. J., 2009, ApJ, 701, L20
Zak E., Tennyson J., Polyansky O. L., Lodi L., Tashkun S. A., Perevalov V. I., 2016, J. Quant. Spectrosc. Radiat. Transfer, 177, 31

SUPPORTING INFORMATION

Additional Supporting Information may be found in the online version of this article:

http://www.mnras.oxfordjournals.org/lookup/suppl/doi:10.1093/mnras/stw1133/-/DC1).

Please note: Oxford University Press is not responsible for the content or functionality of any supporting materials supplied by the authors. Any queries (other than missing material) should be directed to the corresponding author for the article.

This paper has been typeset from a TEX/LATEX file prepared by the author.